https://ntrs.nasa.gov/search.jsp?R=19800023364 2020-03-21T15:53:24+00:00Z

General Disclaimer

One or more of the Following Statements may affect this Document

- This document has been reproduced from the best copy furnished by the organizational source. It is being released in the interest of making available as much information as possible.

- This document may contain data, which exceeds the sheet parameters. It was furnished in this condition by the organizational source and is the best copy available.

- This document may contain tone-on-tone or color graphs, charts and/or pictures, which have been reproduced in black and white.

- This document is paginated as submitted by the original source.

- Portions of this document are not fully legible due to the historical nature of some of the material. However, it is the best reproduction available from the original submission.

Produced by the NASA Center for Aerospace Information (CASI)

9950-316
DOE/JPL 954902 - 80/26
Distribution Category UC - 63

FINAL REPORT TO J.P.L.

for period Oct. 1977 - Mar. 1980

Grant #954902

SILICON SOLAR CELL FABRICATION TECHNOLOGY

Published May 15, 1980

Principal Investigator: O. M. Stafsudd

U. C. L. A.

N80-31871

(NASA-CR-163394) SILICON SOLAR CELL FABRICATION TECHNOLOGY Final Report (California Univ.) 37 p HC A03/MF A01 CSCL 10A

Unclas G3/44 28299

"The JPL Low-Cost Silicon Solar Array Project is sponsored by the U. S. Dept. of Energy and forms a part of the Solar Photovoltaic Conversion Program to initiate a major effort toward the development of low-cost systems.

"This report was prepared as an account of work sponsored by the United States Government. Neither the United States nor the United States Dept. of Energy, nor any of their employees nor any of their contractors, subcontractors, or their employees, makes any warranty, express or implied, or assumes any legal liability or responsibility for the accuracy, completeness or usefullness of any information, apparatus, product or process disclosed, or represents that its use would not infringe privately owned rights."

I. INTRODUCTION

The initial program at U.C.L.A. was to assist J.P.L. during the building and expansion of their laboratory and device fabrication facilities. This work consisted of device fabrication which was composed of the following processing proceedures:

a) low temperature $POCl_3$ diffusions,

b) metalization of back and front ohmic contacts,

c) mask design and fabrication, and

d) sintering in inert and H_2 atmospheres.

These processing steps were varied in accordance with J.P.L.'s instructions.

The device evaluation was performed at U.C.L.A. and J.P.L. The results of these measurements were correlated, and they included such tests as:

a) dark current vs. voltage and log I vs. voltage,

b) light current vs. voltage at AM1 and AMO,

c) capacitance vs. voltage, and

d) spectral response.

The measurements were then interpolated and reduced to determine the material properties such as minority carrier lifetimes (τ_n) and diffusion lengths (L_n). The diffusion lengths determination was accomplished by spectral response measurements at U.C.L.A. Similar measurements of various devices were done by S.P.V. (Surface Photo Voltage method) at J.P.L.

II. MATERIAL CHARACTERIZATION

During the last year and a half, our work has been directed towards the characterization of single and polycrystalline silicon substrates. This work was initially performed by two methods: device fabrication (characterization) and photoconductive lifetime decay measurements. The device characterization of the processed material was accomplished by spectral response measurements determination of I_{sat} and absolute quantum efficiency at a single wavelength (.6328 μm). The results were then reduced to yield the diffusion length of the various samples. The photo-conductive lifetime decay method was implemented in order to determine the minority carrier lifetime in unprocessed wafers.

Previously, photo-conductive decay methods have been difficult and produced indeterminant results due to the limitations in the excitation sources. In our experiments, however, these problems were substantially minimized by the use of a nitrogen pumped dye laser source. The use of a dye laser provided a narrow wavelength band capable of high power pulses at very high repetition rates for the photo-excitation of carriers. Additionally, by selection of various dyes, the wavelength could be varied from 4000 to 7300 Å; this allowed the relative importance of surface recombination effects to be separated from the bulk lifetime.

The photoconductive lifetime decay system is shown in Figure 1. The high powered laser (5 - 50 kw), a National Research Group tuneable dye laser Model NRG-DL-0.03, capable of delivering 60 pulses/sec allowed the use of very small biasing fields (1 - 10 v/cm) across the

ORIGINAL PAGE IS
OF POOR QUALITY

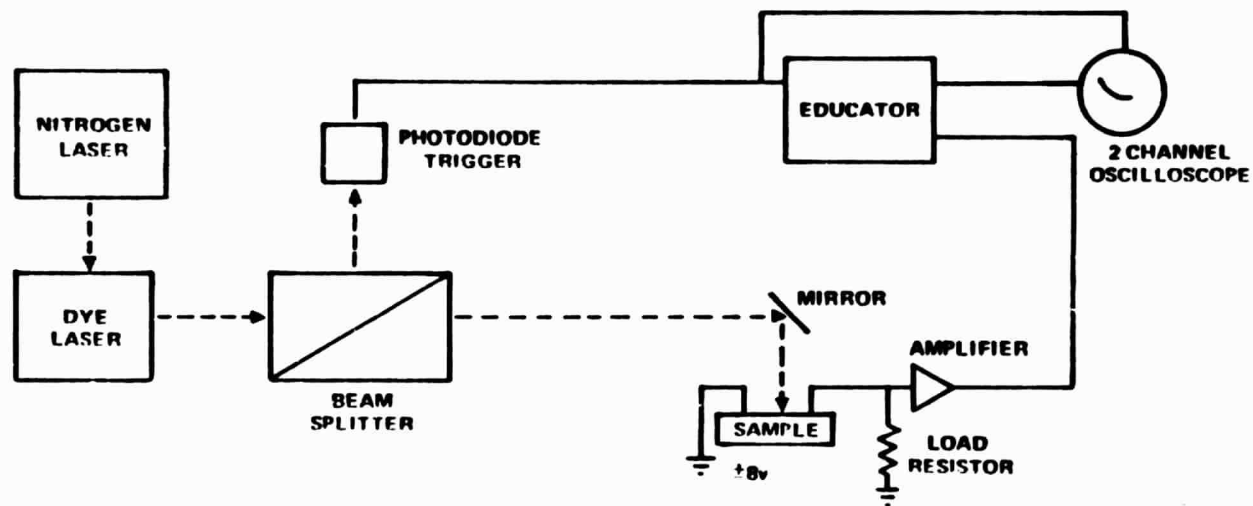

Figure 1. Schematic Setup for the Measurement of Photoconductive Lifetime.

sample. The dye chosen for this experiment was Stilbene 3 which produced a useable range of wavelengths from 4000Å to 5500Å. At these wavelengths, the absorption coefficient for silicon at 23° C is approximately 5.8×10^4 cm^{-1} to $1.2 \times 10^4 cm^{-1}$. This corresponds to an extinction coefficient of approximately 0.16 microns to 0.5 microns. The signal was sampled and held by a P.A.R. eductor model TDH9 and could then be displayed on a Tektronix oscilloscope or x-y recorder. The load resistor was used to match the sample's impedance. The biasing field used was $\pm$8v. This small biasing field is very important for lifetime determination in small grain boundary materials because it eliminates the problem of carrier sweep out due to recombination centers.* In other words, the biasing fields were small enough so that the drift component of the velocity could not move the carriers to a grain boundary in a time period less than the effective minority carrier lifetime. Generally, the photo conductive decay method has experimental problems when the lifetimes are much less than 1μ sec. This is due to the current limitations in the available signal averaging equipment. This is particularly a problem when one considers that a number of polycrystalline materials have diffusion lengths approximately 1-20μ m or corresponding carrier lifetimes of 10^{-10} - 10^{-7} sec.

Due to the problems of the short lifetimes materials, we devised a new method for the measurement of short diffusion lengths. The

---

*It should be noted that the time for a carrier to reach a grain boundary is $\tau_b = \frac{d}{2} \cdot \frac{1}{E\mu}$ where d is the grain dimension, E is the electric field and μ is the mobility. If the sample has a biasing field of approximately 10v/cm, then grain dimensions of approximately 250 microns would have minority carrier residence times of approximately 1μ sec. Therefore any recombination center at the grain boundary will adversely affect lifetime measurements greater than 1μ sec in this case. Much of the poly-silicon measured had grain dimensions on this scale and smaller.

first scheme which was implemented consisted of the excitation by two different wavelengths of an argon ion laser, i.e. the 4880 and 5145 Å lines. In this scheme, the sample was alternatively illuminated by each wavelength using a special chopper and filter system. The relative intensity of the two beams were adjusted until equal by the use of an attenuator. The samples, p-n junction devices, schottky barriers or completely fabricated solar cells with AR coatings, were then illuminated and the short circuit photocurrent was measured. The relative photocurrents generated by the two different wavelengths were then used to calculate the minority carrier diffusion lengths in the sample. The pertinent equations are similar to the MWA equations developed in Appendix A. This method allowed the mapping of the samples' diffusion length. This scheme can also be used for an average diffusion length determination by simply by simply re-focusing the beam to cover the entire surface of the sample.

A shortcoming, however, of the argon laser system was found because of the very short penetration depths of the 4880 and 5145 Å lines. At these wavelengths, the variation in junction depth causes critical errors in the calculation of the diffusion length L_n. This is shown in Figure 2. Additionally, the short penetration depths make accurate determination of diffusion lengths which are longer than 2 microns very difficult. Therefore, the argon ion laser source scheme was replaced by two light emitting diodes (LED's) which were driven 180° out of phase. The wavelengths of the LED's were slightly different but close to 0.9 microns. The longer wavelengths have much deeper penetration depths and are quite useful for the larger values of L_n. In addition, the uncertainities introduced by the

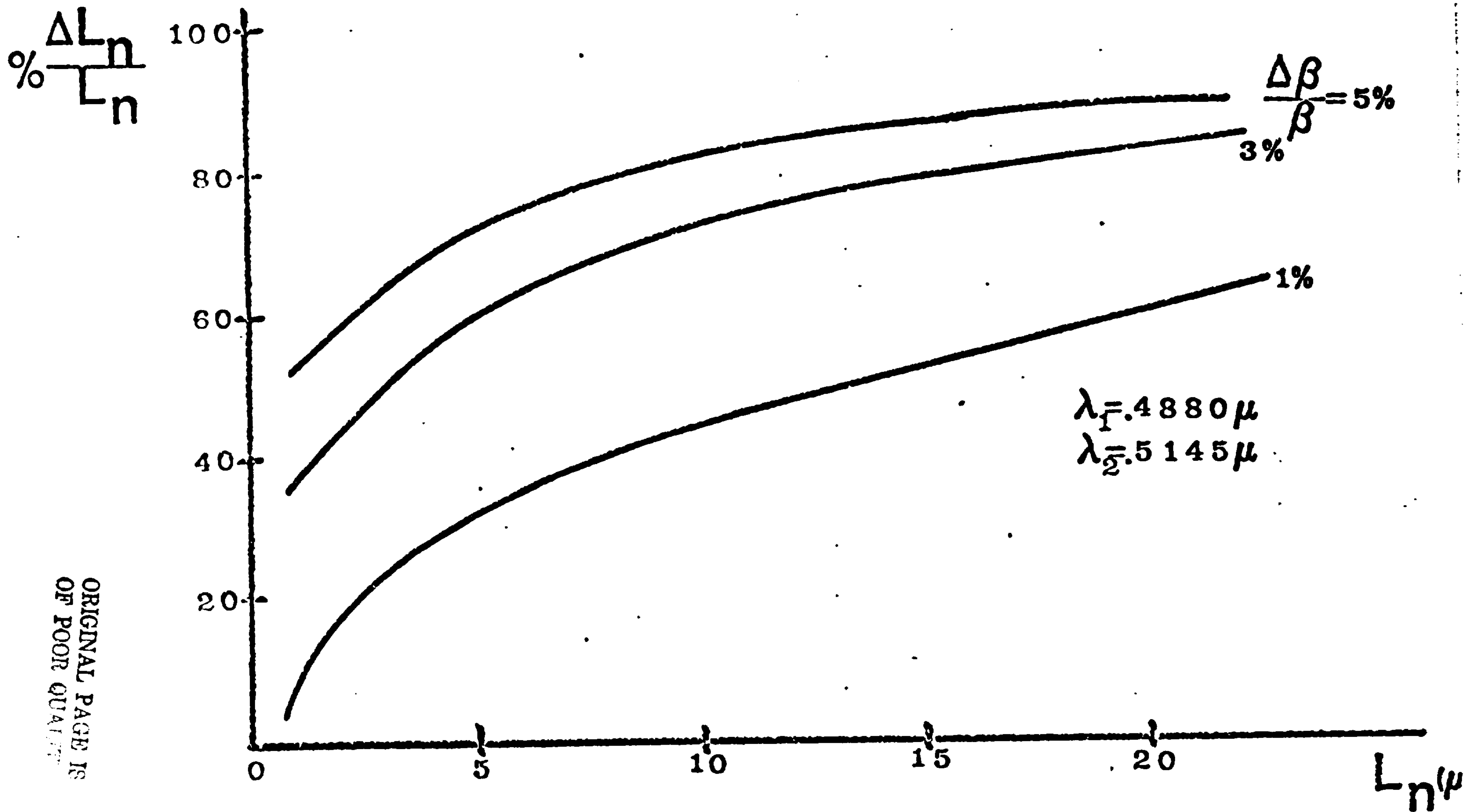

ORIGINAL PAGE IS OF POOR QUALITY

9

FIGURE 2 Theoretical errors in diffusion length due to errors in β for λ = 0.488 and .5145 microns.

variation in junction depth are substantially reduced. This scheme, known as the IR multi-wavelength analyzer (MWA), was presented at the August 1979 PIM Meeting. A complete discussion of the pertinent results follows in Appendix A.

III. DEVICE CHARACTERIZATION

During this contract, solar cells fabricated at J.P.L., U.C.L.A., and various other laboratories in the Low Cost Silicon Solar Array Project were tested at U.C.L.A. The initial tests included the more common techniques such as light and dark current voltage characteristics, Log I vs. V and log I vs log V measurements. The cells were also tested at both AMO and AMI conditions.

Although these tests were quite useful, they were insufficient to characterize the problem associated with devices fabricated in polycrystalline silicon. That is, a poor IV and low efficiency, can result from a large variety of causes in poly-silicon cells. Therefore, it was considered desirable to spacially evaluate these devices. This was accomplished by a laser scanning technique. The devices, solar cells, were placed on an x-y translation stage and illuminated by a laser which was focused to a small, approximately 25 micron, spot size. The short circuit current was measured as a funciton of position using the principal lines of an Argon ion laser, .4880 and .5145 microns, and the helium or neon laser, .638 microns.

Typical scans which were obtained for Wacker solar cell #W-4-4 are shown in Figures 3 and 4. The greatly enhanced structure in the short wavelength scan is typical for polycrystalline cells to the devleopment of the M.W.A. system.

IV. DISCUSSION

The IR MWA system as decribed in Appendix B is a viable diagnostic method for the determination of the quality of the silicon substrate and the effect of processing techniques on the substrate material. However, in practice, data acquisition and reduction are both tedious and overwhelming. For a single 2 cm x 2 cm solar cell, diffusion length evaluations for a 0.1 mm diameter beam would require over 400 separate measurements. Although each individual measurement is simple, the shear number of calculations and measurements are prohibitive.

We are, therefore, automating this scheme with the addition of an Apple II microprocessor. At this time the microprocessor is capable of data acquisition and reduction; however, it does not "command" motion or control the LED source drivers. In the future, we will implement the processor to control all of these functions. The automatic system will be used in the evaluation of various grain boundary passivation studies and the effect of fabrication processing on polycrystalline solar cell material.

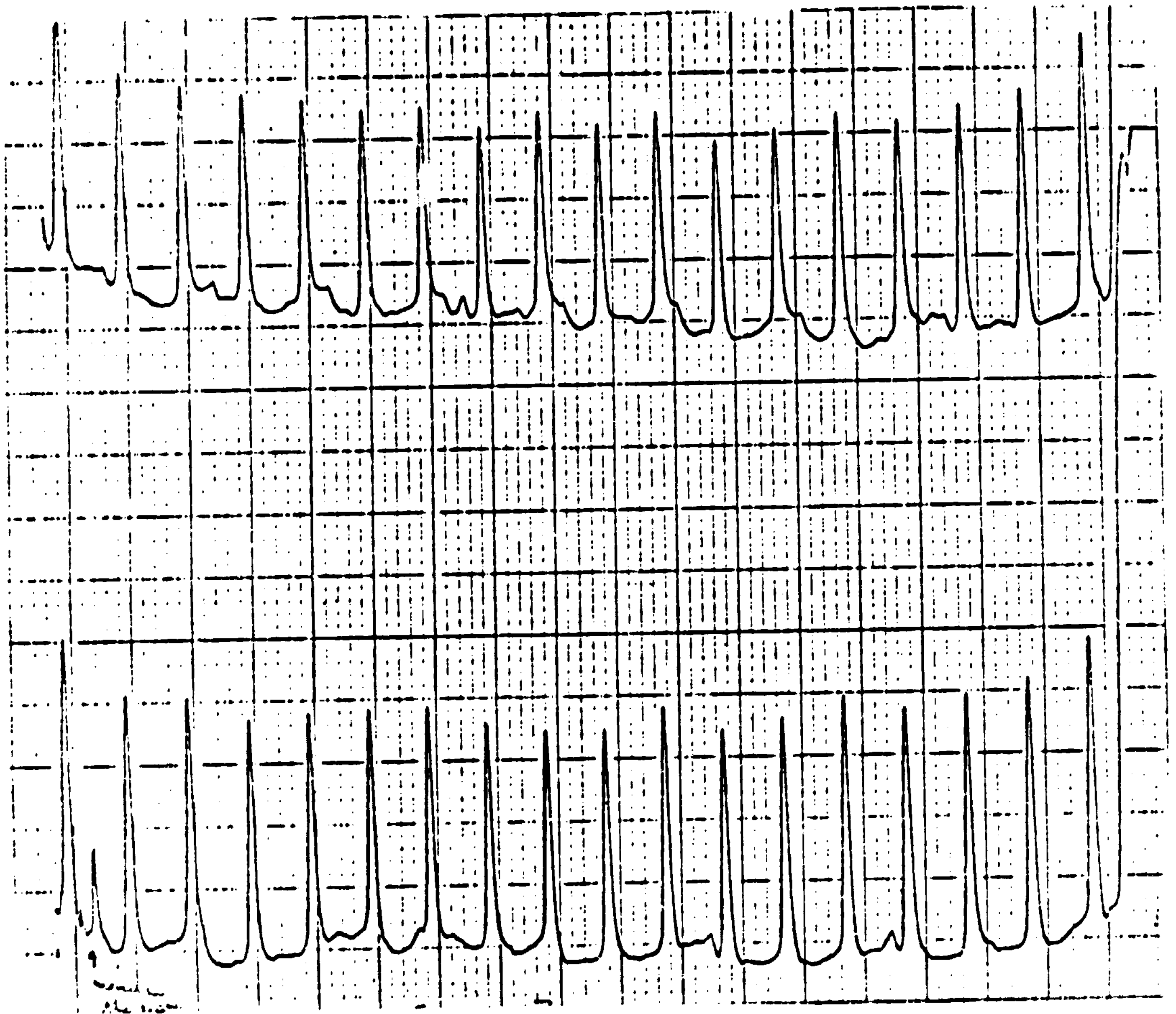

FIGURE 3 CELL # W-4-4 (WACKER) ARGON SCAN

ORIGINAL PAGE IS
OF POOR QUALITY

FIGURE 4 CELL # W-4-4 (WACKER) HeNe SCAN

ORIGINAL PAGE IS
OF POOR QUALITY

APPENDIX A

MULTI-WAVELENGTH ANALYZER FOR DETERMINATION OF DIFFUSION LENGTHS*

O. M. Stafsudd, G. E. Davis and M. Jansen

Electrical Sciences and Engineering Department
University of California
Los Angeles, California 90024

*Work Sponsored under JPL Contract.

ABSTRACT

A new non-destructive method is presented for the determination of the spatial variations in diffusion length due to grain boundary or processing effects. The multi-wavelength analyzer (MWA) requires the measurement of the short circuit current generated by two or more infrared LED's operating at different wavelengths. Using the ratio of current differences generated at each wavelength (A.C. component) to the average current generated (D.C. component), the diffusion length may be determined within the limitations of the absorption coefficient used. The short circuit current is generated over the surface area related to the spot size of the focused LED's which is typically 0.5 mm. By mounting the sample on a translation table, it is possible to scan across the sample and determine the point-to-point variations in the diffusion length. This method can be used to evaluate pre-processed materials as well as devices after p-n junction fabrication. Therefore, it allows a quantitative evaluation of the influence of fabrication techniques.

Polycrystalline silicon solar cells were measured by the MWA method. This method showed spacial variation in polycrystalline diffusion lengths more than an order of magnitude from point-to-point for RTR polycrystalline silicon solar cells. The average value of the diffusion length is, however, in good agreement with the SPV measurements on the same 4 cm^2 device. Because the technique is based on ratios, the effects of carrier generation in the surface "dead layer" and changes in reflectivity from point to point are reduced to a second order correction.

ORIGINAL PAGE IS
OF POOR QUALITY

I. INTRODUCTION

An important parameter which determines the solar cell performance is the minority carrier diffusion length (L_n) in the base or substrate region. The diffusion length influences the short circuit current and, therefore, the overall efficiency (η) of the solar cell. Several methods (1-7) have been developed to measure the diffusion length. Some of these methods are destructive and do not generally allow for the point-by-point determination of the diffusion length. The spatial resolution is particularly important in the assessment of polycrystalline base solar cells. The reduction of the overall efficiency in these cells is a result of the grain boundaries which produce high recombination velocities and shortened effective diffusion lengths.

The multi-wavelength analyzer was developed as a new method for the testing of solar cells. It is simple and easily lends itself to on-line testing of terrestial solar cells and/or materials. The method is based on the short circuit current generated by a solar cell at two or more wavelengths. The generation of excess carriers is due to 2 LED's operating at different wavelengths modulated 180° out-of-phase as shown in Figure 1. The carriers are generated within the localized area illuminated by the LED beams and are collected by the junction. The cell is scanned by moving the sample on a translation table at a constant rate. This scanning allows a point-by-point determination of the diffusion length. The spatial resolution is limited by the focused beam size on the sample which is typically 0.5mm in diameter in the present system. This spot size can be further reduced if desired by the use of additional

optics; however, the resulting reduction of generated currents would require additional processing.

Due to the nature of the MWA, the evaluation of L_n is possible before processing by fabricating a simple schottky barrier and removing it before diffusion and device fabrication. The diffusion lengths can then be determined as a function of position and compared to the pre-processed values. Therefore, the effect of various processing steps on the diffusion length can be determined quantitatively (8).

II. MWA System Design

The multi-wavelength analyzer is schematically shown in Figure 2. The LED's which operate at 2 different IR wavelengths are driven in a pulsed mode 180° out-of-phase. The LED's are independently adjustable with respect to intensity and positioning and are mounted vertically on an optical rail perpendicular to each other with a (40-60) beam splitter in the optical path. The beams are optically focused to approximately 0.5mm. The solar cell or schottky device is mounted on a translation table which is driven by a motor in the x-direction with the position determined by a transducer. The solar cell is operated in a short circuit mode and the output is sent to a Keithley 480 picoammeter. The voltage output of the picoammeter is fed to a PAR 124A Lock-in amplifier which is referenced to the LED driver. The lock-in signal can be read directly or displayed on an x-y recorder.

ORIGINAL PAGE IS
OF POOR QUALITY

III. Theoretical

The geometry of the solar cell is shown in Figure 3. The devices analyzed in this work are assumed to have a shallow diffused junction and furthermore, the surface layer, 0 to $-x_j$ is assumed to have a negligible minority carrier lifetime. Therefore, all carriers generated in this region are neglected leaving only the generated term g as an effective source of excess carriers. Under these assumptions, the steady state minority carrier distribution for a monochromatic generation can be expressed as

$$D \frac{d^2 n}{dx^2} - \frac{n}{\tau_b} + F_o \alpha e^{-\alpha x} = 0 \qquad (1)$$

where D is the minority carrier diffusion constant,

n is the excess minority carrier concentration,

τ_b is the minority carrier lifetime,

F_o is the photon flux density, and

α is the absorption coefficient.

Solving for the minority carrier concentration n and substituting into the expression for the short circuit current density $J_{sc} = qD \left.\frac{dn}{dx}\right|_o$, we obtain after some manipulation:

$$J_{sc} = q \frac{F_o \alpha L_n}{1-\alpha^2 L_n^2} \left\{ \frac{\cosh W/L_n - e^{-\alpha W} - \alpha L_n \sinh W/L_n}{\sinh W/L_n} \right\} . \qquad (2)$$

For W > $_n$,

$$J_{sc} = \frac{qF_o \ \alpha L_n}{1+ \ \alpha L_n} . \qquad (3)$$

where $F_o = e^{-\alpha x_j}$ (1-r) F_i and r is the surface reflectivity coefficient and F_i is the incident photon flux. Thus, for small αL_n, we obtain the short circuit generated at λ_1 as

$$I_{sc_1} = \frac{qe^{-\alpha_1 x_j} F_{1i} \ (1-r_1)\alpha_1 L_n}{1+\alpha_1 L_n} \qquad (4)$$

Likewise, we may find the short circuit current due to the generation at λ_2 as

$$I_{sc_2} = \frac{qe^{-\alpha_2 x_j} F_{2i} \ (1-r_2)\alpha_2 L_n}{1+\alpha_2 L_n} \qquad (5)$$

Defining R as the ration $\frac{I_{AC}}{I_{DC}}$, we obtain

$$R = 2\frac{\left(I_{sc_1} - I_{sc_2}\right)}{I_{sc_1} + I_{sc_2}} \qquad (6)$$

Thus, solving Equation (6) for the diffusion length yields

$$L_n = \frac{1}{\alpha_1 \alpha_2} \left[\frac{\alpha_1 (2-R) - \alpha_2 \beta (2+R)}{R-2 + \beta (2+R)} \right] \quad (7)$$

where β is a function of the photon fluxes, transmissivity and absorption terms at λ_1 and λ_2 and is expressed as

$$\beta = B \frac{1-r_2}{1-r_1} e^{-\left(\alpha_2 - \alpha_1\right) x_j} \quad (8)$$

where

$$B = \frac{F_{1i}}{F_{2i}}$$

It should be noted that this method as exhibited in Equation (7) is based on the difference in absorption coefficients, $(\alpha_1 - \alpha_2)$, times the thickness of the diffused layer, d. In the case of a single wavelength method, the effective exponential factor is the product of αd. Therefore, the single wavelength measurements are much more sensitive to junction depth variations. An equivalent argument can also be expressed for the reflectivity errors in the single wavelength methods versus those obtained in the MWA method.

IV. Calibration and Error Analysis

There are five factors which contribute errors in the calculation of diffusion lengths as determined by the MWA. They are the LED spectral distribution, the calibration of the photon flux, the variation of the reflection coefficient, uncertainties in the absorption coefficient, and the variation in the junction depth. The effect of each of these contributing errors and their effect on the diffusion length measurement is discussed below.

A. LED Spectral Distribution

The accuracy of this method depends upon the determination of the absorption coefficient for the wavelengths used and, therefore, the wavelengths of emission must be accurately known. The LED's were supplied with nominal peak emission wavelengths of 880 and 930 nanometers. Figure 4 shows the actual spectral distribution of the LED's used. The peak wavelengths were 907 and 955 nanometers, respectively.

B. Calibration of the Photon Flux

It is necessary to know the relative photon fluxes at the two different wavelengths. This can be accomplished by two methods. In the first method, a thermal detector (thermopole), which is wavelength independent in this spectral region, is positioned at the sample location. The relative driving currents of the two LED are adjusted to null the A.C. signal from the thermopole. Under this nulling

condition, the two LED's are supplying equal powers to the test cell, and, therefore, $B = \lambda_2/\lambda_1$.

In the second method, the LED drive is adjusted to produce a known relative photon flux and therefore a known B. This can be accomplished by using a PIN photo diode of known quantum efficiency at the two wavelengths. The photo diode is substituted for the test solar cell and the A.C. signal is nulled. Under these conditions, $B=\eta_2/\eta_1$, where η_1 is the quantum efficiency at λ_1 and η_2 is the quantum efficiency at λ_2. The drift in the null was found to be only $1:10^3$ over a period of 20 minutes. The effect of this 0.1% drift or any other inaccuracy in the determination of β with respect to the measurement of L_n is shown in Figure 5.

C. Determination of Reflection Coefficients.

The sample was mounted on the translation table with a 30° tilt introduced. The reflection coefficient was established by using the reflected signal from the solar cell surface as the input to a PIN photodiode and measuring the ratio of reflected current of the solar cell to the incident current.

It should be noted that variations in the ratio of reflective coefficients at the two LED wavelengths produce the same error effect as variations in β. If the cell is covered by an anti-reflective coating, it is necessary to take this into account when spacial variations in the relative reflectivities are encountered.

D. Absorption Coefficient.

As shown in Equation (6), the choice of absorption coefficient (α) is quite important to the determination of L_n. The best absorption

coefficients as a function of wavelength have been established experimentally by Runyan[9] and Dash[10] for stress relieved and non-stress relieved Si. In the case of small grain polycrystalline silicon, the non-stress relieved α was used. The α is established by

$$\alpha^{-1} = (-1.06964 + 3.34982\,\lambda^{-1} - 3.61649\lambda^{-2} + 1.34831\lambda^{-3})\ \mu m^{-1} \quad (a)$$

In general, there is no exact determination of α, however, the error introduced into L_n due to errors in α are shown in Figure 6.

ORIGINAL PAGE IS
OF POOR QUALITY

E. Junction Depth.

The junction depth is determined from the diffusivity of the material and the time used to grow the epi-layer. Generally, the thickness is kept to within .1 - .2μ to minimize losses at short wavelengths. The errors introduced in the determination of L_n from improper junction depth data are shown in Figure 7.

V. Experimental Results

The MWA was used to study a series of RTR (Motorola Laser Recrystalized Ribbon) polycrystalline solar cells. These cells were supplied by the Jet Propulsion Laboratory, Pasadena. J.P.L. had previously determined the cell efficiencies and the average L_n by the Surface Photovoltage method (SPV). Figures 8 to 10 show I_{sc_1}, I_{sc_2} and I_{ac} for sample S872B3 as a function of position on the surface. Equations 6 and 7 are used to determine the diffusion lengths as a function of position along the sample. These scans show that there is a substantial variation in L_n across the poly-

crystalline samples. In some cases, L_n varies by a factor of 10 or more from point-to-point. However, the average effective diffusion length determiend for the three samples compares favorably with the SPV measurements as shown in Table 1.

Figure 11 shows the structural characteristics of sample S872B3 which were revealed by etching in a 25 HF: 18 HNO_3: 5 CH_3COOH: 10 H_2O by volume with a 1 g $Cu(NO_3)_2$ in 58 cc of the etching solution. The sample exhibits a highly unordered crystalline structure containing twins, dislocations and high angle grain boundaries. The picture is a composite of photo micrographs. There are some unavoidable changes in contrast from section to section. These are not meaningful structurally but rather represent limitations in the photographic equipment. The MWA measured diffusion lengths are noted on the photograph. The dots indicate the center of the measurement area in each case. The number is the effective diffusion length measured in micro meters. It can be seen that there is considerable correlation between gross features in the photomicrograph and low diffusion lengths. But, the low L_n near or inside regions of poor crystallinity cannot be directly attributed to grain boundary effects, precipitates or selective segregation of unwanted impurities without further investigation. It is interesting to note, however, that, in general, the diffusion length along the direction of crystalization varies only by a factor of 2 while perpendicular to this direction, factors of 30 or more are encountered.

VI. Conclusions

It should be noted that in the MWA method the parameter that is determined is $L_n \cdot \alpha$, that is the absorption coefficient-diffusion length product. The usefullness of this method relies heavily upon the independent determination of the absorption coefficient. H wever, any material whose absorption coefficients are known can be measured by this method if a photo-barrier device can be produced.

The MWA is a useful non-destructive technique for the determination of the minority carrier diffusion length as a function of position. It can be easily automated to do multiple linear scans across the entire solar surface

Acknowledgements

We would like to thank Gary Pollack of the Jet Propulsion Laboratory for his assistance.

REFERENCES

1. Mahan, J. E., T. W. Ekstedt, R. I. Frank, R. Kaplow, IEEE Transactions on Electron Devices, Vol. 26, pp. 733-739, 1979.

2. Stokes, E. D. and T. L. Chu, Applied Physics Letters, Vol. 30, pp. 425-426, 1977.

3. Bell, R. O. and G. N. Freedman, 12th IEE Photovoltaic Specialists Conference, pp. 89-94, 1978.

4. Chu, T.L. and E. D. Stokes, 12th IEEE Photovoltaic Specialists Conference, pp. 95-99, 1978.

5. Reynolds, J. H. and A. Meulenberg, Journal of Applied Physics, Vol. 45, pp. 2582-2592, 1974.

6. Neugroschell, A., P. Chen, S. C. Pao, and F. A. Lindholm, IEEE Transactions on Electron Devices, Vol. 25, pp. 485-590, 1978.

7. V. G. Weizer, 9th IEEE Photovoltaic Specialists Conference, p. 67, 1975.

8. Stafsudd, O. M., G. E. Davis and M. Jansen, to be published.

9. Runyan, W. E., Southern Methodist University Report, SMU 83-13, 1967.

10. Dash, W. C. and R. Newman, Physical Review, Vol. 99, pp. 1151-1155, 1955.

LIST OF CAPTIONS

Fig. 1 LED modulated outputs and solar cell short circuit AC and DC current.

Fig. 2 Schematic of Multi Wavelength Analyzer.

Fig. 3 Geometry used for solar cell.

Fig. 4 Spectral distribution of LED showing peak at .907 μm and .955 μm.

Fig. 5 Theoretical errors in diffusion length due to errors in β.

Fig. 6 Theoretical errors in diffusion length using stressed to unstressed absorption coefficient.

Fig. 7 Theoretical errors in diffusion length due to 50% error in junction depth for x_j = .1 and .15 μm.

Fig. 8 MWA scan at position B across sample S872B3.

Fig. 9 MWA scan at position E across sample S872B3.

Fig. 10 MWA scan at position H across sample S872B3.

Fig. 11 Defects revealed in etched silicon wafer with diffusion lengths indicated.

Table 1 Comparison between averaged MWA and SPV values of diffusion length for various samples.

ORIGINAL PAGE IS
OF POOR QUALITY

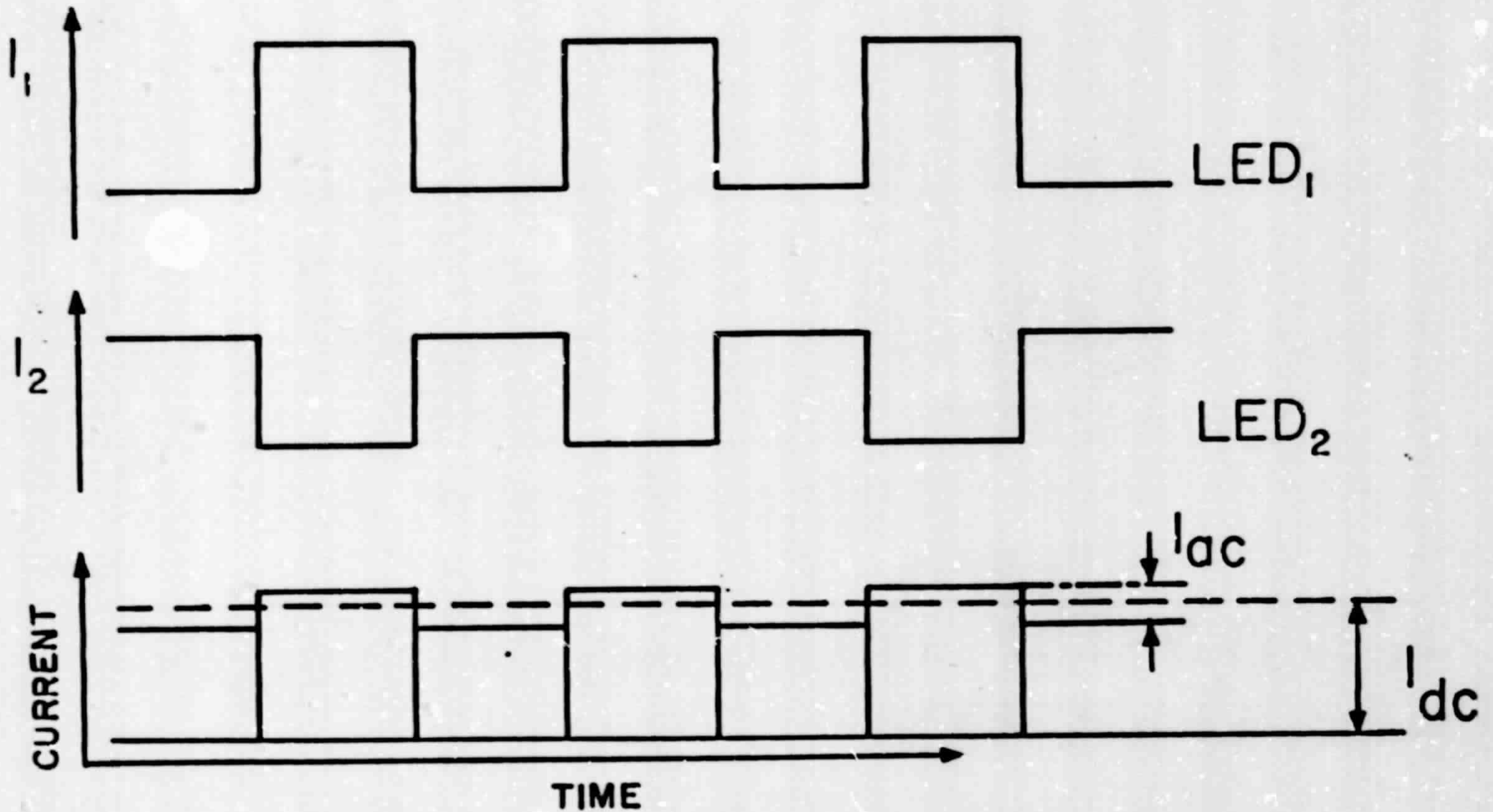

Figure 1. LED modulated outputs and solar cell short circuit AC and DC currents.

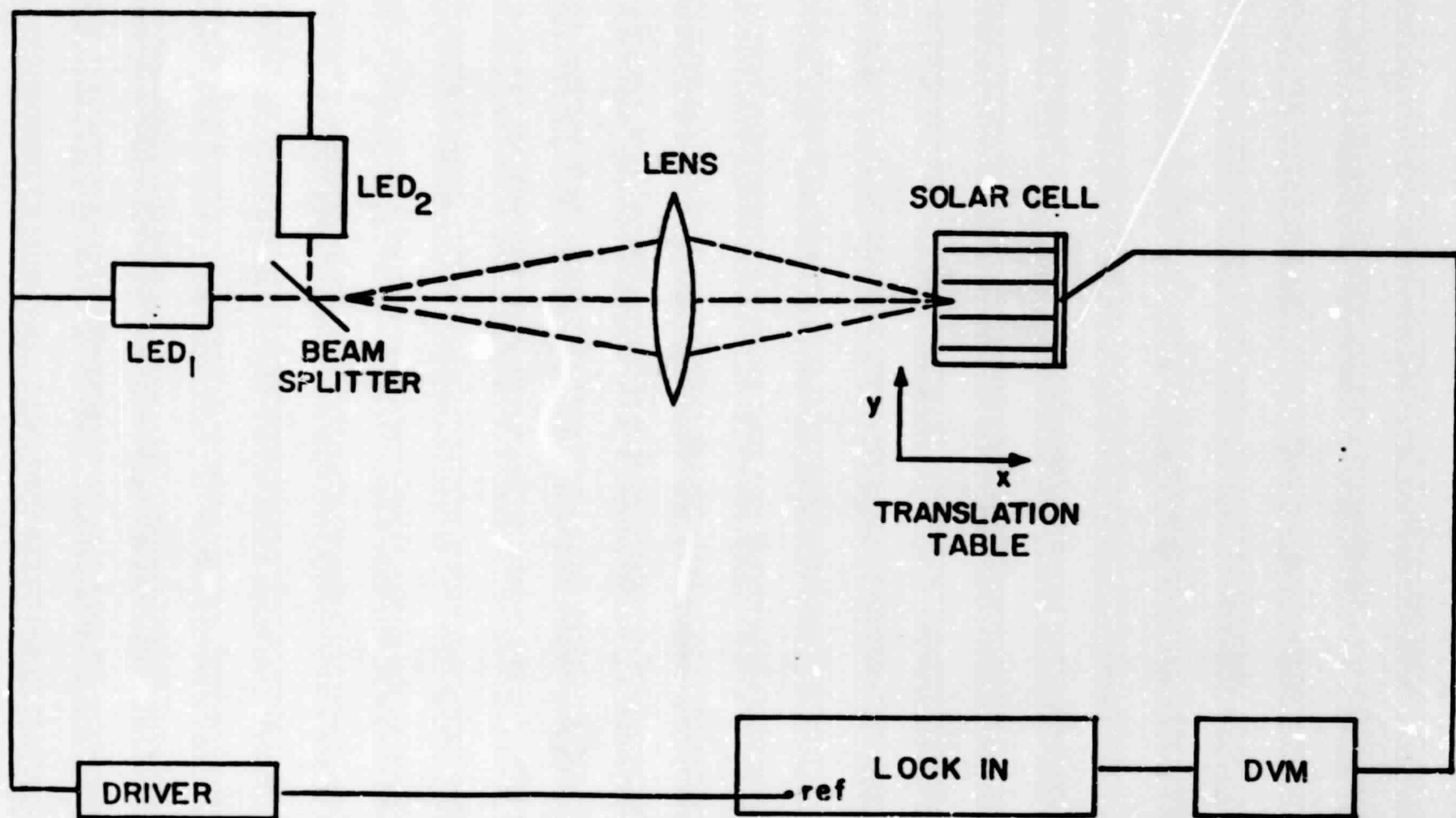

Figure 2. Schematic of Multi Wavelength Analyzer.

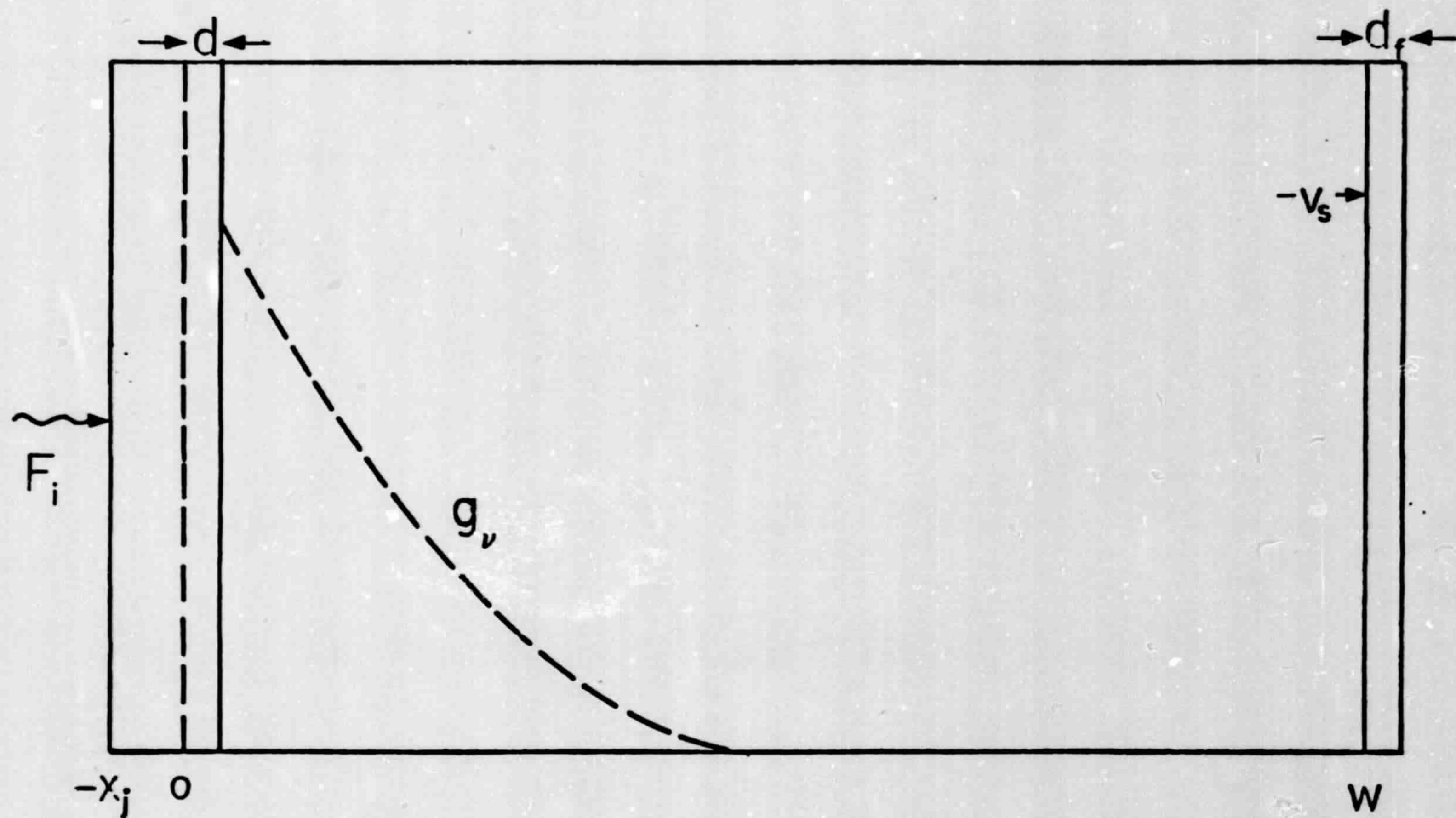

Figure 3. Geometry used for solar cell.

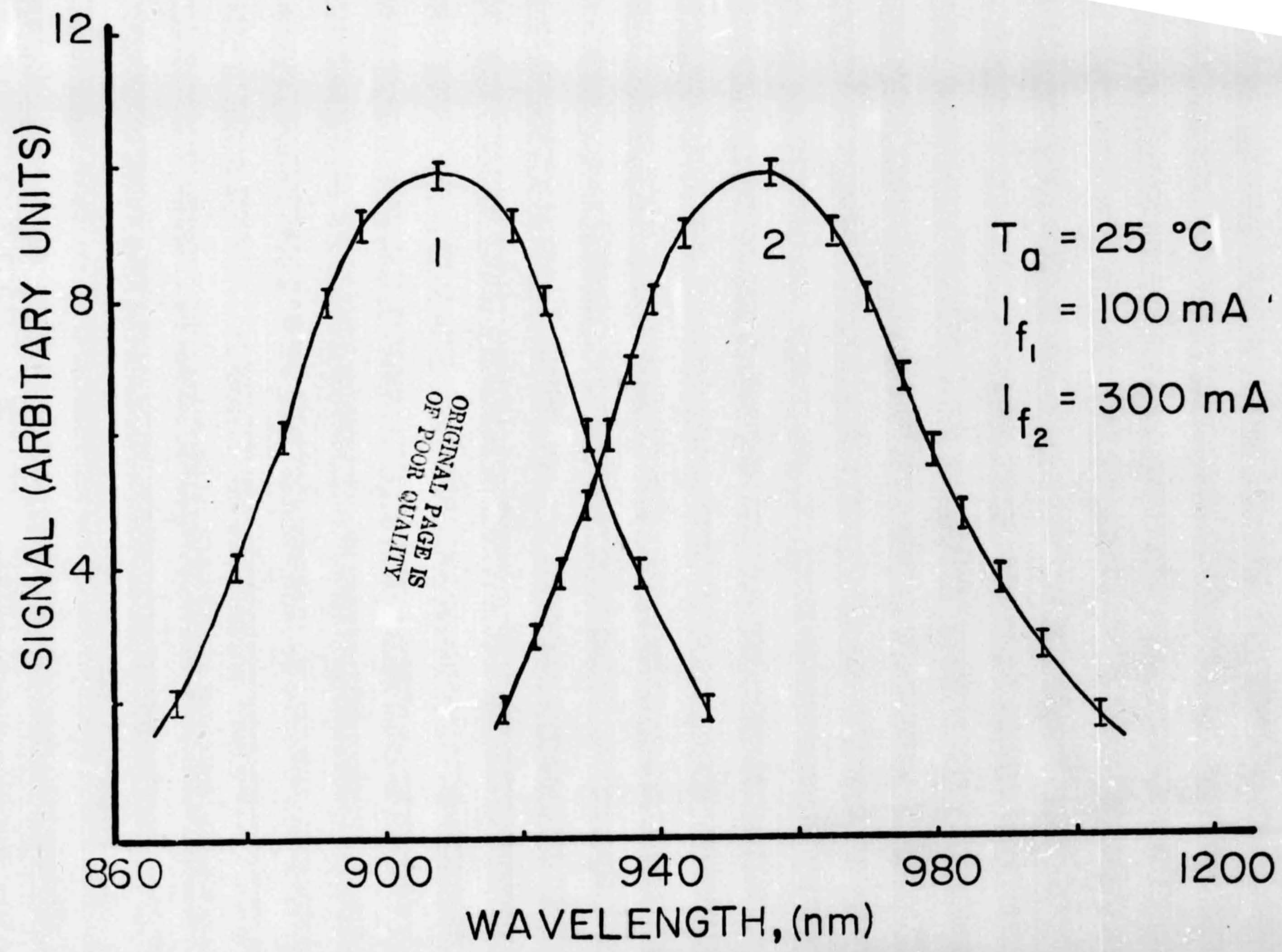

ORIGINAL PAGE IS
OF POOR QUALITY

Figure 4. Spectral distribution of LEDs showing peaks at 0.907 μm and 0.955 μm.

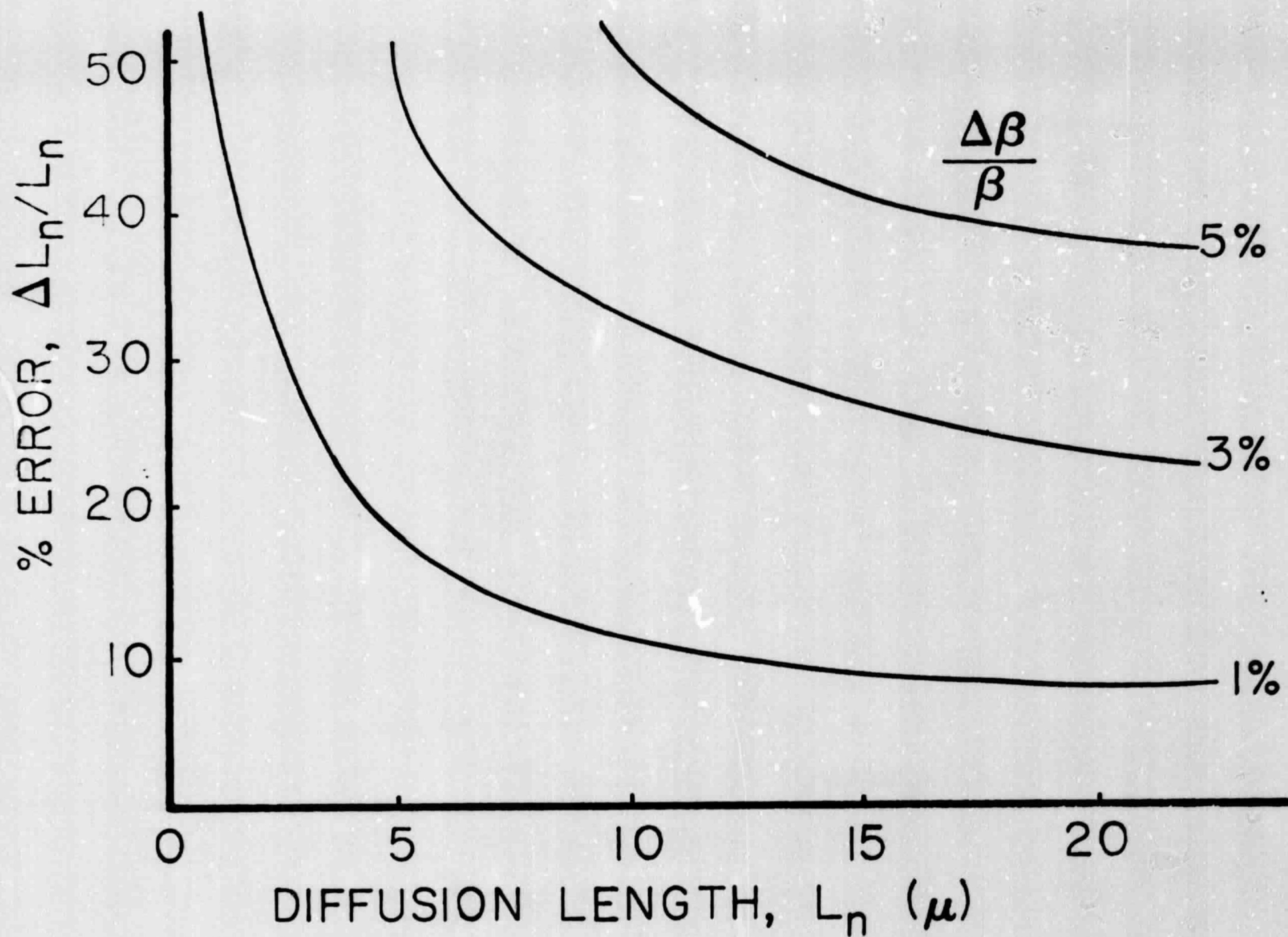

Figure 5. **Theoretical errors in diffusion length due to errors in β.**

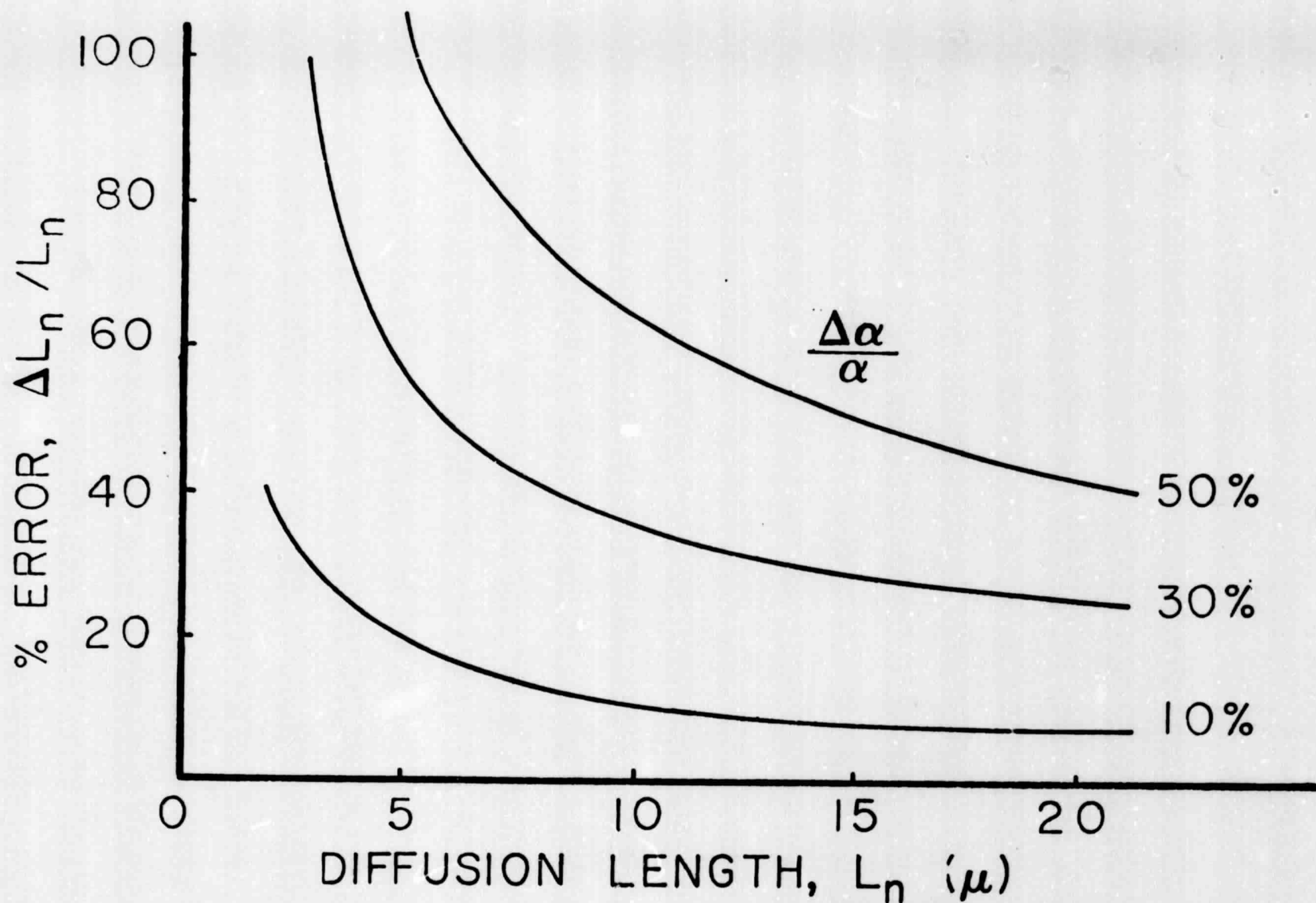

Figure 6. Theoretical errors in diffusion length for stressed and unstressed absorption coefficients.

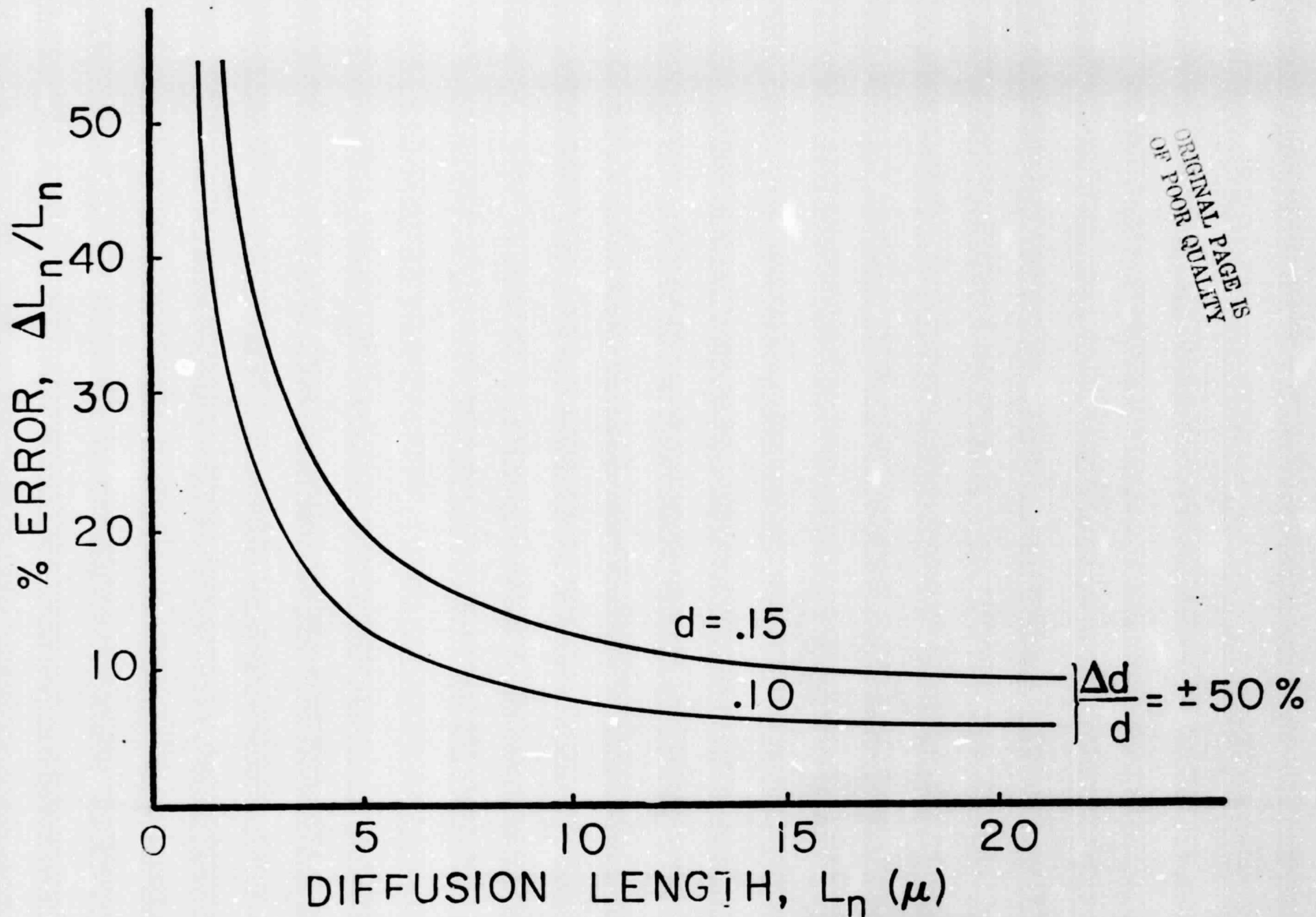

ORIGINAL PAGE IS
OF POOR QUALITY

Figure 7. Theoretical errors in diffusion length due to 50% error in junction depth for x_j = .1 and .15 microns.

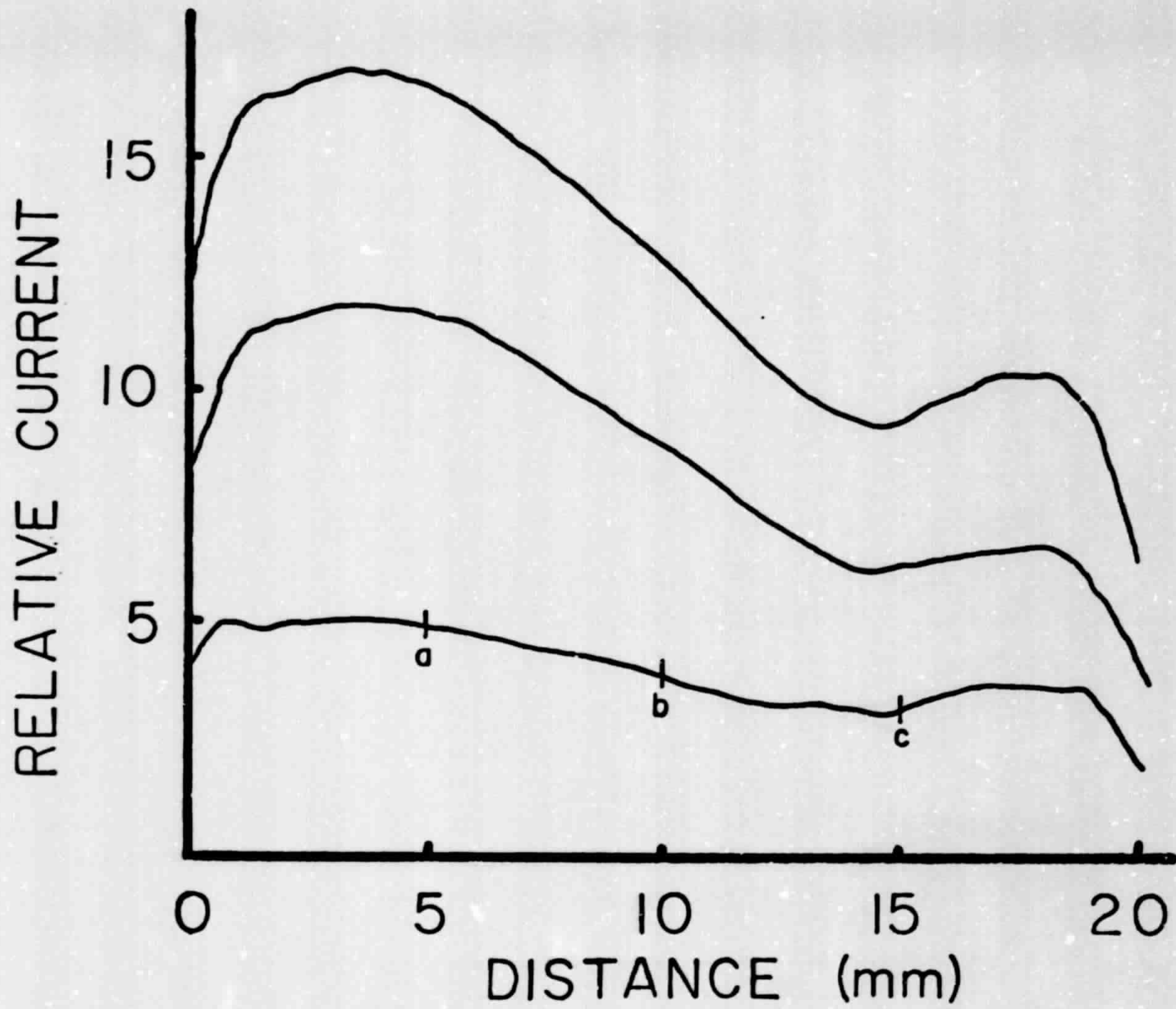

Figure 8. MWA scan at position B across sample S872B3.

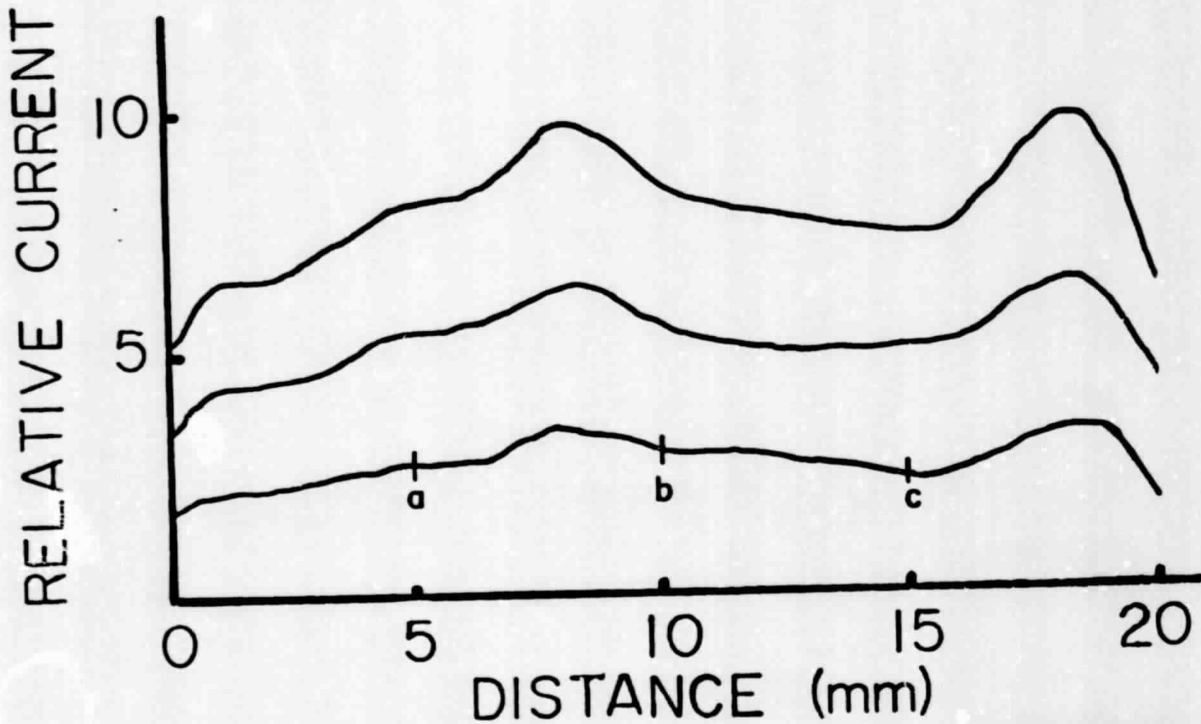

Figure 9. MWA scan at position E across sample S872B3.

ORIGINAL PAGE IS
OF POOR QUALITY

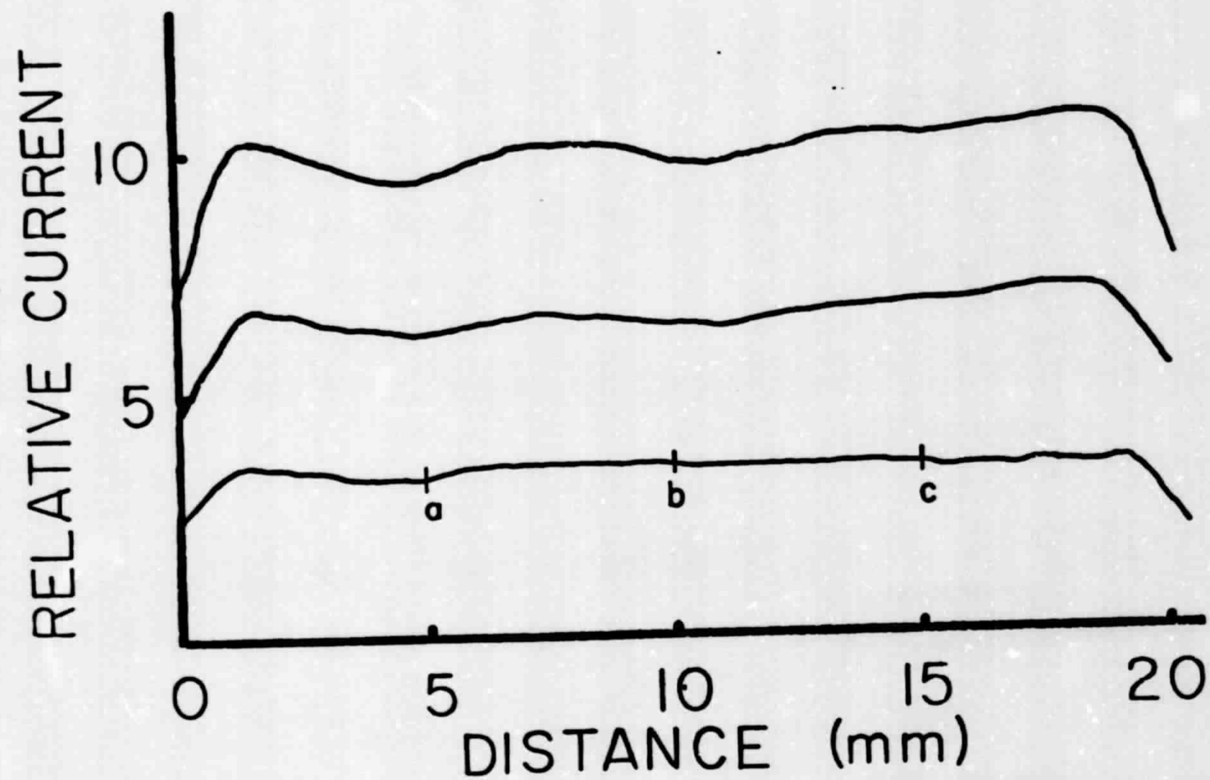

Figure 10. MWA scan at position H across sample S872B3.

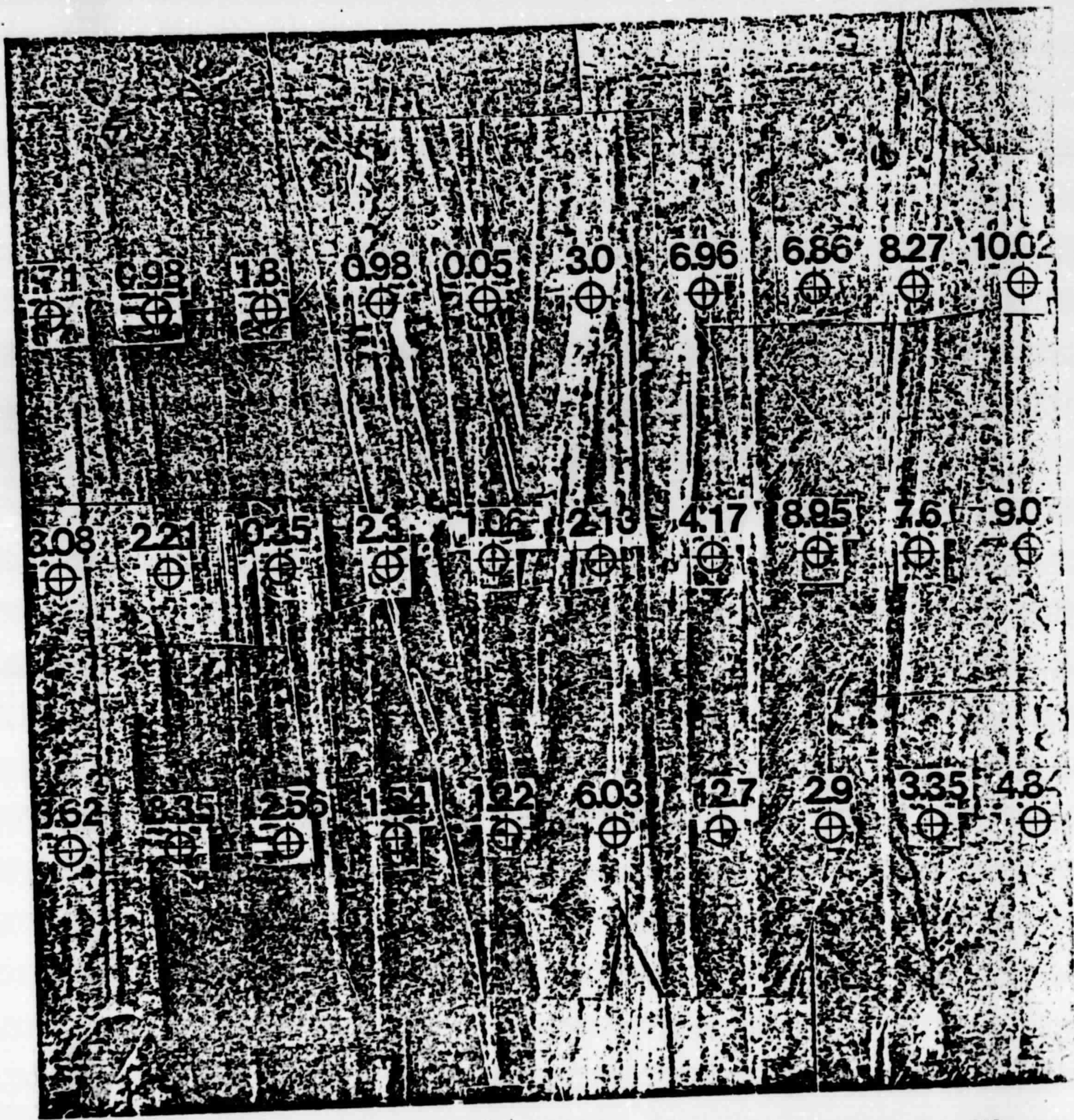

Figure 11. Defects revealed in etched silicon sample S872B3 with diffusion lengths indicated.

ORIGINAL PAGE IS
OF POOR QUALITY

TABLE 1

Comparison between averaged MWA and SPV values of diffusion length for various samples.

Sample ID	Cell Material	Cell Efficiency	Scan #	Position	MWA $L_n(\mu)$	MWA $L_n(\mu)$	SPV $L_n(\mu)$
869-1	CVD, Not Annealed	4.0%	7A	a	2.18	3.02	2.6
				b	1.42		
				c	1.26		
			7B	a	1.42		
				b	3.42		
				c	2.36		
			7C	a	5.02		
				b	4.73		
				c	6.13		
S872B3	Single Crystal Not Annealed	4.5%	8A	a	10.02	4.12	2.8
				b	9.07		
				c	4.84		
			8B	a	8.27		
				b	7.6		
				c	3.35		
			8C	a	6.86		
				b	8.95		
				c	2.9		
			8D	a	6.96		
				b	4.17		
				c	12.7		
			8E	a	3.0		
				b	2.13		
				c	6.03		
			8F	a	0.05		
				b	1.06		
				c	1.22		
			8G	a	0.98		
				b	2.3		
				c	1.54		
			8H	a	1.80		
				b	0.35		
				c	2.56		
			8I	a	0.98		
				b	2.21		
				c	3.35		
			8J	a	1.71		
				b	3.08		
				c	3.62		
838B3	CVD, Annealed	0.9%	9A	a	3.9	3.81	4.0
				b	1.64		
				c	3.72		
			9B	a	3.9		
				b	1.64		
				c	3.72		
			9C	a	4.18		
				b	4.27		
				c	5.33		